# Dual spin nodal box structure in ternary ferromagnet $K_3NiCl_6$ with broad topological surface states

Yang Li[1,2,*]

[1] Aviation and Automobile School, Chongqing Youth Vocational & Technical College, Chongqing, China.

[2] College of Physics, Chongqing University, Chongqing, China.

[*] Emails: liyang@cqwu.edu.cn

## Supplementary materials

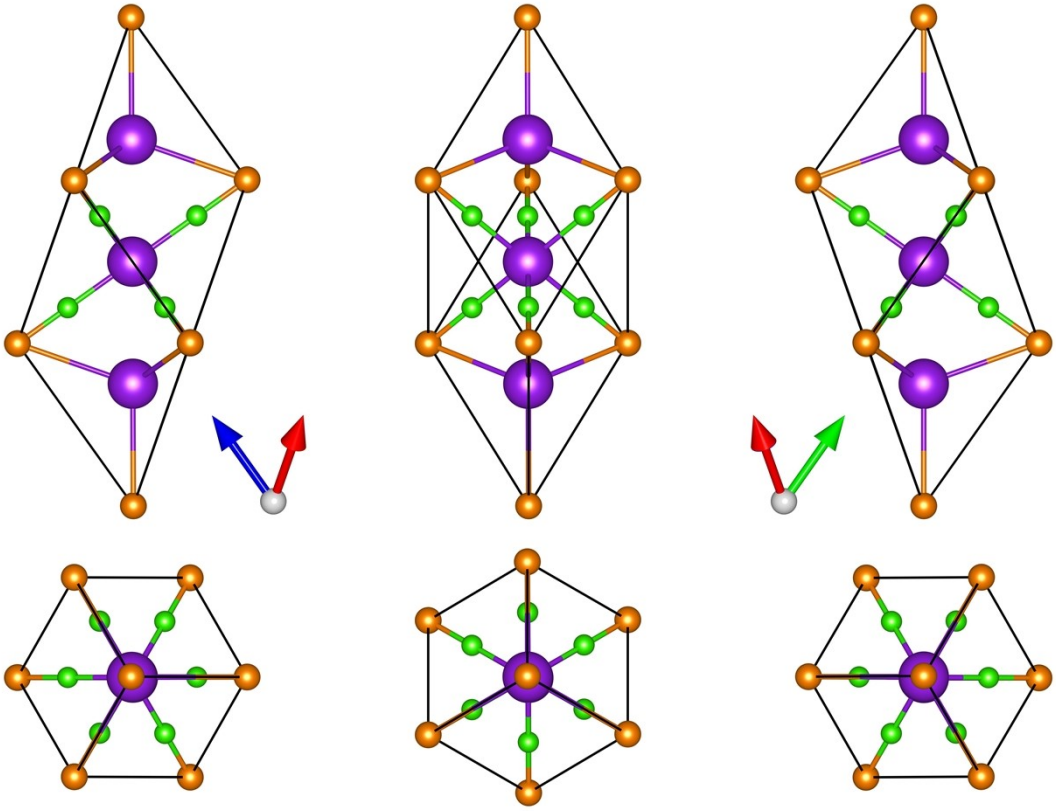

Figure S1: The primitive cell for the ternary ferromagnetic compound $K_3NiCl_6$ under different view directions.

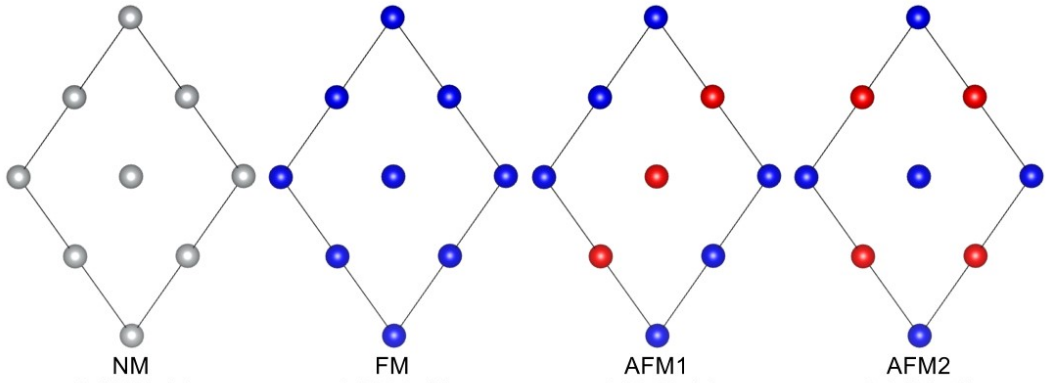


Figure S2: The determination of the magnetic ground state. Four magnetic configurations have been considered within the 2×2×1 super cell for the ternary compound $K_3NiCl_6$, including a nonmagnetic state (NM), a ferromagnetic state (FM), and two antiferromagnetic states (AFM1 and AFM2).

Table S1: The calculated total energy for the ternary compound $K_3NiCl_6$ under different magnetic configurations and Hubbard U values, including a nonmagnetic state (NM), a ferromagnetic state (FM), and two antiferromagnetic states (AFM1 and AFM2). All units are in eV.

| U | NM | FM | AFM1 | AFM2 |
|---|---|---|---|---|
| 0 | -129.92650387 | -130.37598263 | -130.33907432 | -130.36583783 |
| 1 | -127.53794896 | -128.25866331 | -128.20413630 | -128.23976407 |
| 2 | -125.18643464 | -126.25504395 | -126.18571625 | -126.23018987 |
| 3 | -122.87266109 | -124.39084332 | -124.30830860 | -124.36164512 |
| 4 | -120.59756899 | -122.69169927 | -122.59702055 | -122.65917156 |
| 5 | -118.36243350 | -121.17672655 | -121.07046360 | -121.14217675 |
| 6 | -116.16845808 | -119.85908214 | -119.82164481 | -119.73963995 |

Table S2: The calculated total and local magnetic moments and coupling parameters for the ternary compound $K_3NiCl_6$ under different Hubbard U values.

| U | $M_{total}$ | $M_K$ | $M_{Ni}$ | $M_{Cl}$ | $J_1$ | $J_2$ |
|---|---|---|---|---|---|---|
| eV | $\mu_B$ | | | | meV | |
| 0 | 0.9994 | 0.0000 | 0.7060 | 0.0333 | 0.59518 | 2.58896 |
| 1 | 0.9996 | 0.0000 | 0.8000 | 0.0590 | 0.90311 | 2.71722 |
| 2 | 1.0000 | 0.0000 | 0.9120 | 0.0480 | 0.92082 | 2.59736 |
| 3 | 0.9995 | 0.0000 | 1.0390 | 0.0440 | 0.83576 | 2.37550 |
| 4 | 1.0000 | 0.0000 | 1.1730 | 0.0630 | 0.73327 | 2.14900 |
| 5 | 0.9998 | 0.0000 | 1.3050 | 0.0810 | 0.63122 | 1.97976 |
| 6 | 0.9908 | 0.0000 | 1.4340 | 0.0990 | 0.56502 | 1.86005 |

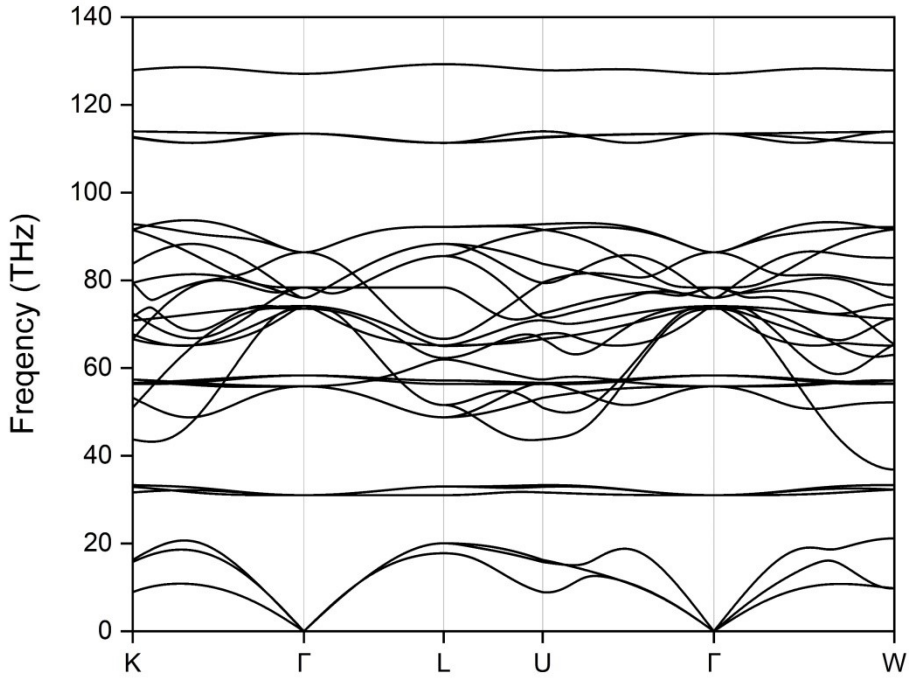


Figure S3: The calculated phonon spectrum for the ternary compound $K_3NiCl_6$.

Table S3: The calculated various elastic constants ($C_{11}$, $C_{12}$, and $C_{44}$), Young's modulus (E), shear modulus (G), and Poisson's ratio (ν) for the ternary compound $K_3NiCl_6$.

| $C_{11}$ | $C_{12}$ | $C_{44}$ | E | G | B | ν |
|---|---|---|---|---|---|---|
| (GPa) | | | | | | |
| 41.299 | 17.739 | 9.616 | 27.548 | 10.430 | 25.593 | 0.321 |

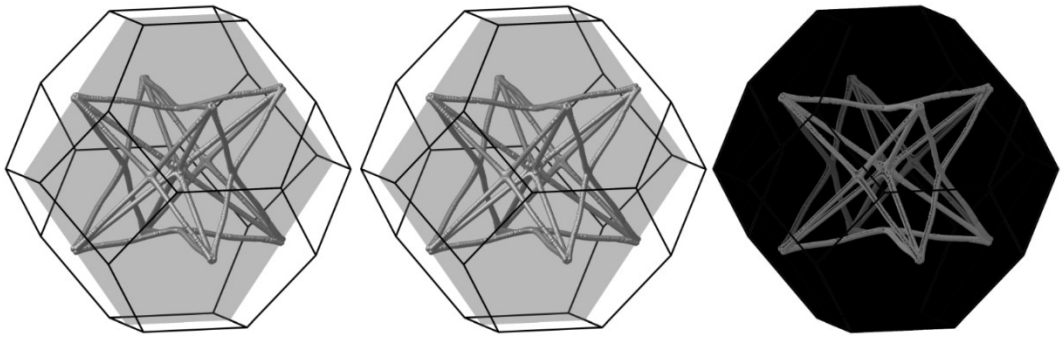

Figure S4: The nodal box distributions in the two spin channels and their difference in the Brillouin zone. The gray scale is applied to provide the same color reference for better comparison. The slight white color in the right panel with most of black color indicates the difference between the two spin channels.

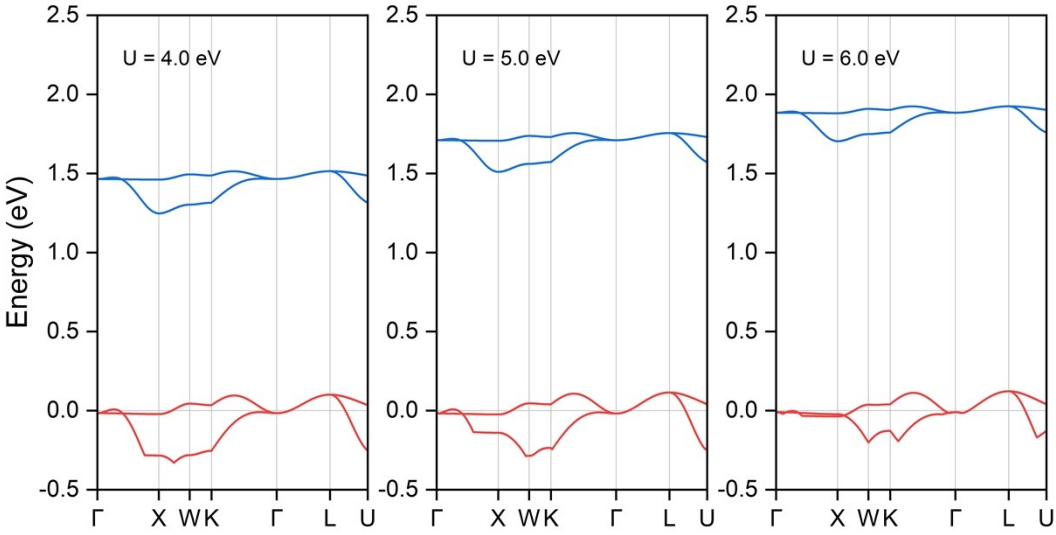


Figure S5: The local band structure in both spin channels along the Γ-X-W-K-Γ-L-U path for ternary ferromagnetic compound $K_3NiCl_6$ under DFT+U method. The Fermi energy level is shifted to 0 eV, as indicated by the horizontal line. Hubbard U values ranging from 4 to 6 eV were employed to accommodate strong Coulomb interactions. Only the bands related to the spin nodal box are shown.

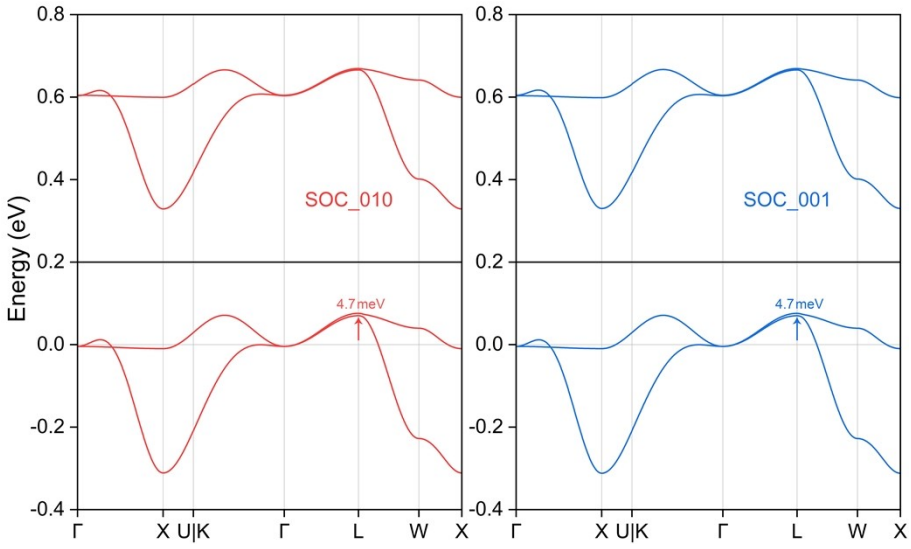


Figure S6: The calculated local band structure along the Γ-X-W-K-Γ-L-U path for ternary ferromagnetic compound $K_3NiCl_6$ under [010] and [001] magnetization directions. The Fermi energy level is shifted to 0 eV, as indicated by the horizontal line. The maximum opened band gap is situated at the L point, with the corresponding gap value explicitly indicated.

Table S4: The calculated total energy (eV) under different magnetization directions with different Hubbard U corrections. The red color indicates the ground energy state.

| U | $E_{001}$ | $E_{010}$ | $E_{100}$ | $E_{110}$ | $E_{101}$ | $E_{011}$ | $E_{111}$ |
|---|---|---|---|---|---|---|---|
| 0 eV | -32.62037829 | -32.62037791 | -32.62037873 | -32.62037806 | -32.62037815 | -32.62037780 | -32.62037709 |
| U | $E_{001}$ | $E_{010}$ | $E_{100}$ | $E_{110}$ | $E_{101}$ | $E_{011}$ | $E_{111}$ |
| 1 eV | -32.08976873 | -32.08976834 | -32.08976835 | -32.08976819 | -32.08976848 | -32.08976838 | -32.08976668 |
| U | $E_{001}$ | $E_{010}$ | $E_{100}$ | $E_{110}$ | $E_{101}$ | $E_{011}$ | $E_{111}$ |
| 2 eV | -31.58731477 | -31.58731472 | -31.58731519 | -31.58731576 | -31.58731582 | -31.58731589 | -31.58731229 |
| U | $E_{001}$ | $E_{010}$ | $E_{100}$ | $E_{110}$ | $E_{101}$ | $E_{011}$ | $E_{111}$ |
| 3 eV | -31.11977134 | -31.11977149 | -31.11977218 | -31.11977194 | -31.11977192 | -31.11977176 | -31.11976735 |
| U | $E_{001}$ | $E_{010}$ | $E_{100}$ | $E_{110}$ | $E_{101}$ | $E_{011}$ | $E_{111}$ |
| 4 eV | -30.69358290 | -30.69358308 | -30.69358617 | -30.69358058 | -30.69358145 | -30.69358147 | -30.69357441 |
| U | $E_{001}$ | $E_{010}$ | $E_{100}$ | $E_{110}$ | $E_{101}$ | $E_{011}$ | $E_{111}$ |
| 5 eV | -30.31365378 | -30.31365164 | -30.31365459 | -30.31364610 | -30.31364599 | -30.31364619 | -30.31364104 |
| U | $E_{001}$ | $E_{010}$ | $E_{100}$ | $E_{110}$ | $E_{101}$ | $E_{011}$ | $E_{111}$ |
| 6 eV | -29.98338469 | -29.98338037 | -29.98338447 | -29.98338381 | -29.98338186 | -29.98338109 | -29.98337895 |

Table S5: The calculated total magnetic moment ($\mu_B$) under different magnetization directions with different Hubbard U corrections.

| U | $M_{001}$ | $M_{010}$ | $M_{100}$ | $M_{110}$ | $M_{101}$ | $M_{011}$ | $M_{111}$ |
|---|---|---|---|---|---|---|---|
| 0 eV | 1.0011 | 1.0011 | 1.0011 | 0.7079 | 0.7079 | 0.7079 | 0.5780 |
| U | $M_{001}$ | $M_{010}$ | $M_{100}$ | $M_{110}$ | $M_{101}$ | $M_{011}$ | $M_{111}$ |
| 1 eV | 1.0004 | 1.0004 | 1.0004 | 0.7074 | 0.7074 | 0.7074 | 0.5776 |
| U | $M_{001}$ | $M_{010}$ | $M_{100}$ | $M_{110}$ | $M_{101}$ | $M_{011}$ | $M_{111}$ |
| 2 eV | 0.9997 | 0.9997 | 0.9997 | 0.7069 | 0.7069 | 0.7069 | 0.5772 |
| U | $M_{001}$ | $M_{010}$ | $M_{100}$ | $M_{110}$ | $M_{101}$ | $M_{011}$ | $M_{111}$ |
| 3 eV | 0.9994 | 0.9994 | 0.9994 | 0.7067 | 0.7067 | 0.7067 | 0.5770 |
| U | $M_{001}$ | $M_{010}$ | $M_{100}$ | $M_{110}$ | $M_{101}$ | $M_{011}$ | $M_{111}$ |
| 4 eV | 1.0002 | 1.0002 | 1.0002 | 0.7072 | 0.7072 | 0.7072 | 0.5774 |
| U | $M_{001}$ | $M_{010}$ | $M_{100}$ | $M_{110}$ | $M_{101}$ | $M_{011}$ | $M_{111}$ |
| 5 eV | 1.0037 | 1.0035 | 1.0037 | 0.7096 | 0.7096 | 0.7096 | 0.5795 |
| U | $M_{001}$ | $M_{010}$ | $M_{100}$ | $M_{110}$ | $M_{101}$ | $M_{011}$ | $M_{111}$ |
| 6 eV | 1.0110 | 1.0108 | 1.0110 | 0.7148 | 0.7147 | 0.7147 | 0.5835 |

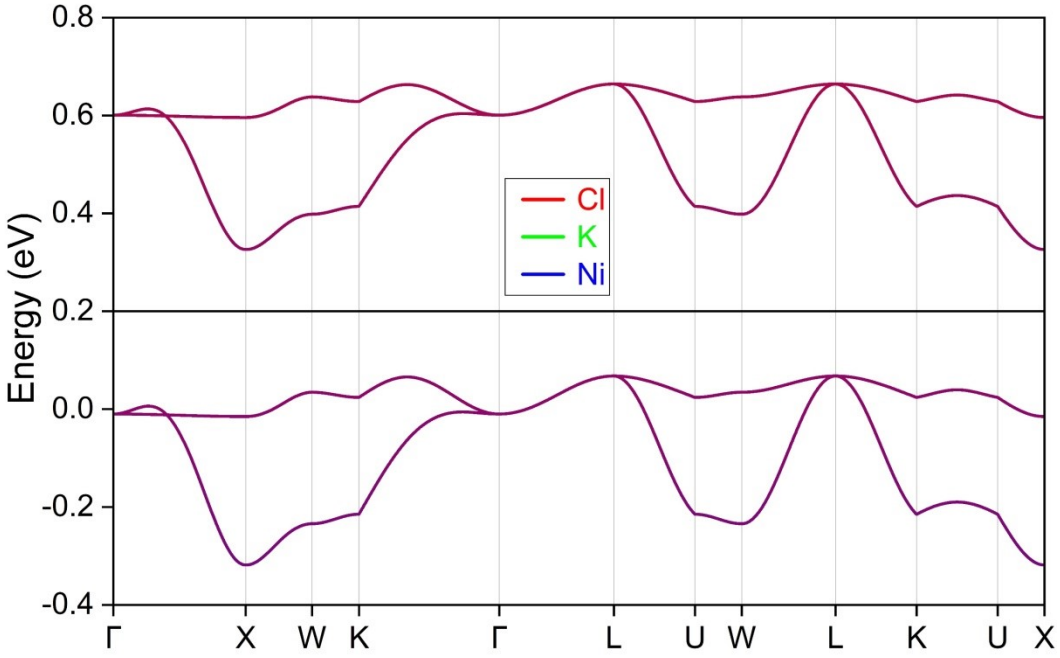


Figure S7: The projection for the two bands related to the spin nodal box structure in both spin channels. The line color is weighted with the different element contributions.

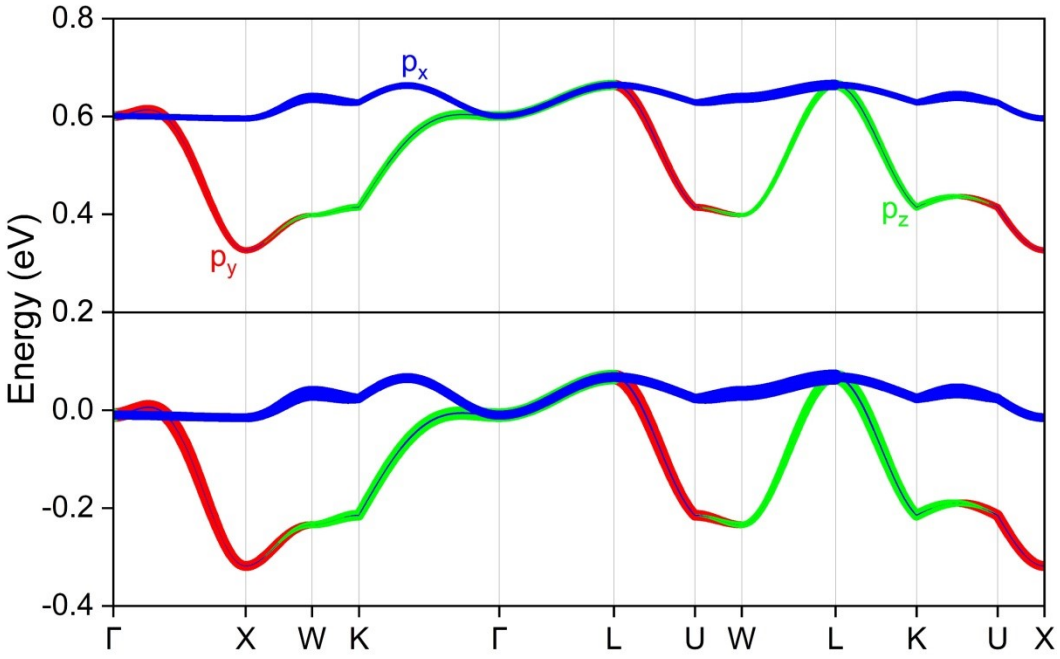


Figure S8: The orbital projection for the two bands related to the spin nodal box structure. Only the major contributions from the p orbital of Cl elements are selected and shown.

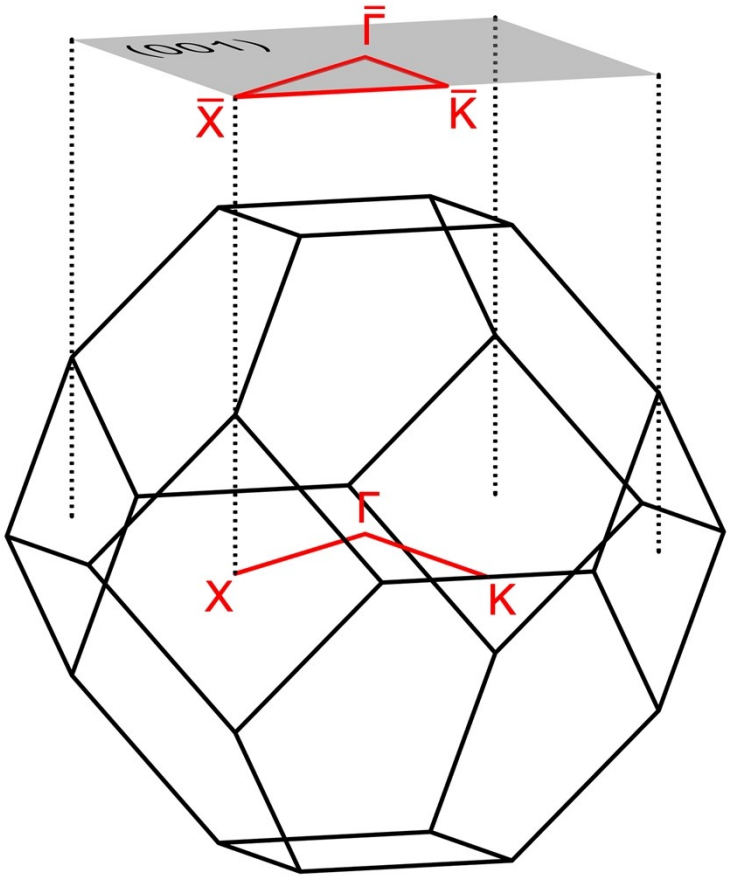


Figure S9: The (001) surface Brillouin zone and the high symmetry points and paths, with correspondence from the bulk Brillouin zone.

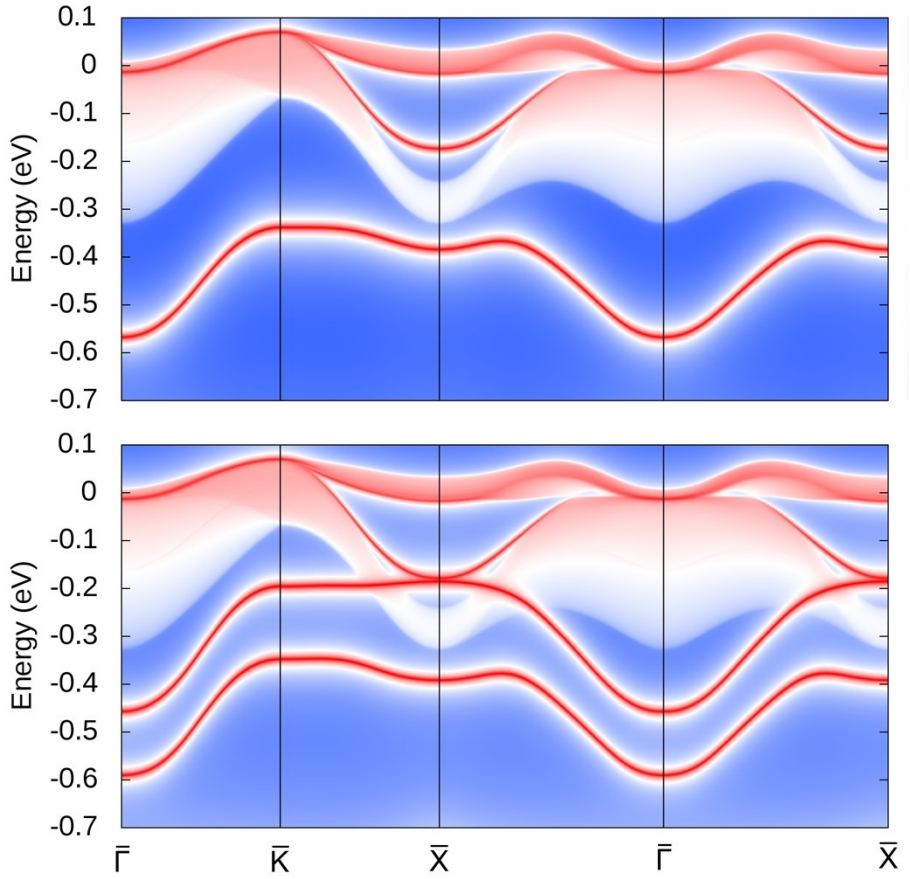


Figure S10: The (001) surface band spectrum for the ternary ferromagnetic compound $K_3NiCl_6$ in the spin-up channels with extended energy scale. The extra surface states with floating behavior are from the trivial obstructed boundary states.

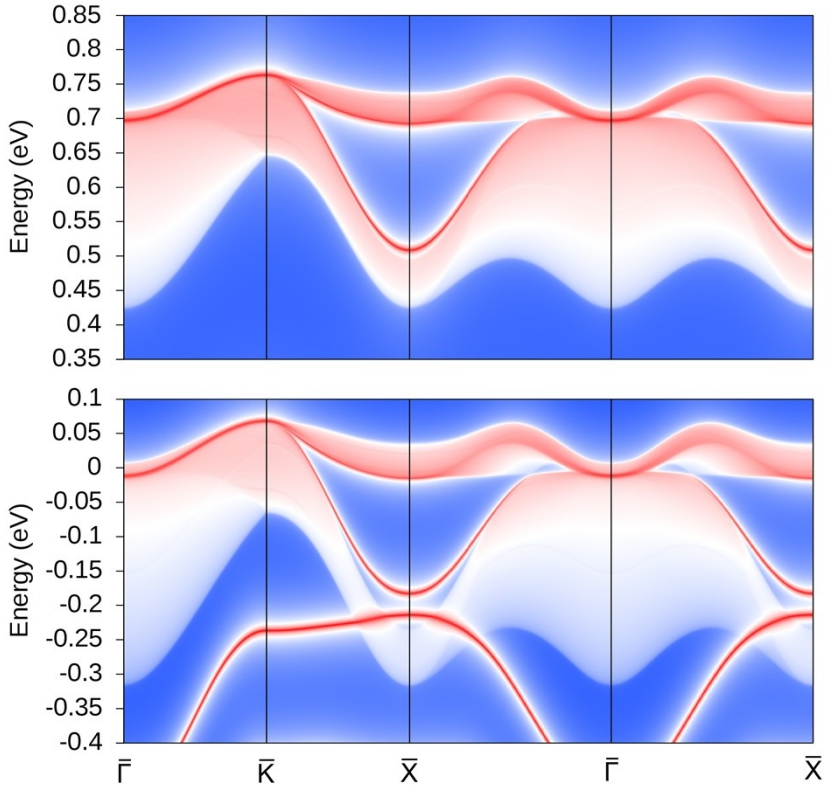


Figure S11: The (001) surface band spectrum for the ternary ferromagnetic compound K3NiCl6 under [010] magnetization direction.

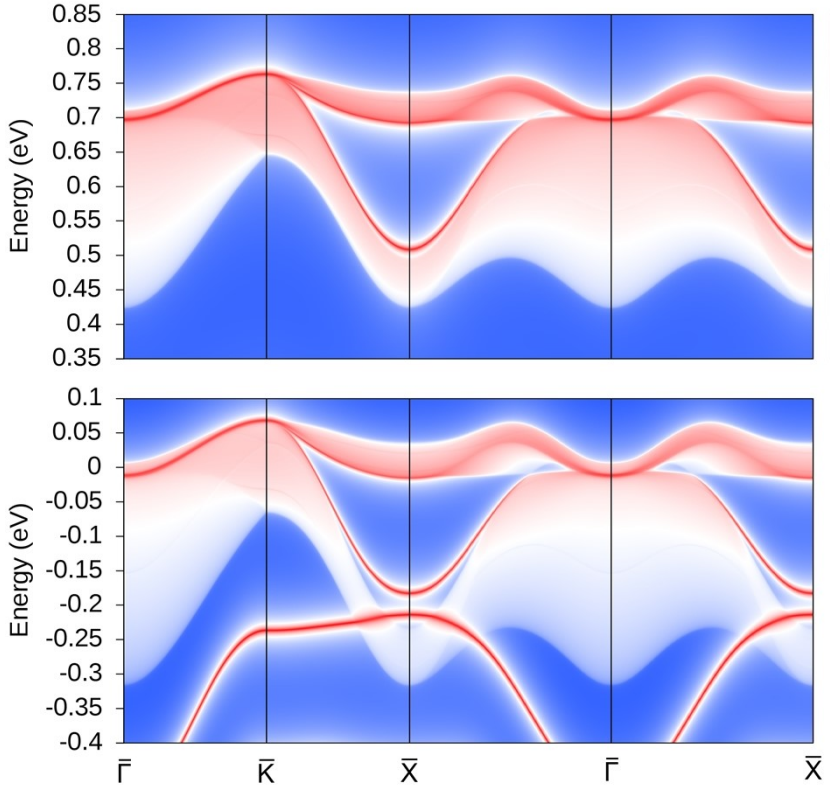


Figure S12: The (001) surface band spectrum for the ternary ferromagnetic compound K3NiCl6 under [001] magnetization direction.